EJNMMI Physics

ORIGINAL RESEARCH Open Access

Motion study on upright patient positioning in walk-through PET: evaluation in a clinical setting

Rabia Aziz[1*], Florence Marie Muller[1,2], Nadia Withofs[3], Jens Maebe[1], Meysam Dadgar[1,4], Boris Vervenne[1], Yves D'Asseler[5], Christian Vanhove[1] and Stefaan Vandenberghe[1]

*Correspondence:
Rabia Aziz
rabia.aziz@ugent.be
[1]Department of Electronics and Information Systems, Ghent University, Corneel Heymanslaan 10, 9000 Ghent, Belgium
[2]Physics and Instrumentation Group, Department of Radiology, University of Pennsylvania, 3620 Hamilton Walk, Philadelphia, PA 19104, USA
[3]Division of Nuclear Medicine and Oncological Imaging, Department of Medical Physics, CHU of Liege, Quartier Hopital, Avenue de L'Hopital, 1, 4000 Liege, Belgium
[4]Radiology, Stanford University, California, CA, USA
[5]Department of Nuclear Medicine, Ghent University Hospital, C. Heymanslaan 10, Ghent, Belgium

Abstract

Background The novel upright walk-through PET (WT-PET) scanner enhances patient throughput compared to the conventional cylindrical PET systems but introduces unique challenges related to patient motion. This study evaluates the rigid body motion of the head, shoulders, chest, and abdomen of patients standing in a WT-PET mock-up scanner, focusing on ergonomic features, including a headrest and hand supports, designed to minimize motion during upright imaging. To contextualize these findings, a patient study using a conventional PET scanner was conducted, along with a control healthy volunteer study involving both WT-PET and conventional PET systems.

Methods Motion data were collected from 30 patients positioned on the WT-PET, 13 patients scanned with a conventional cylindrical PET, and 12 healthy volunteers scanned with both systems. Infrared markers placed at anatomical positions tracked three-dimensional marker positions during 30-s periods of normal breathing and breath-hold instructions in the WT-PET mock-up. Conventional PET scans for patients and healthy volunteers involved 8-min acquisitions. Motion was quantified by calculating the Euclidean distance (ED) of the markers' 3D centroids.

Results In WT-PET patients, breath-holding significantly reduced mean abdominal motion by 24%, with mean ED decreasing from 2.31 ± 1.32 mm during normal breathing to 1.76 ± 0.81 mm during breath-holding. While only 30% of patients completed a full 30-s breath hold, 80% maintained breath holds longer than 20 s. Age was significantly correlated with increased head motion during normal breathing, whereas body mass index and gender showed no significant effects. Compared with WT-PET healthy volunteers, patient motion on the WT-PET was over three times higher for the head (0.47 ± 0.13 mm vs. 1.51 ± 2.32 mm) and 36% higher for the abdomen (1.70 ± 0.63 mm vs. 2.31 ± 1.32 mm). Relative to patients in conventional PET, WT-PET patients showed slightly lower head motion (1.55 ± 1.05 mm vs. 1.51 ± 2.32 mm), but abdominal motion was 44% lower in WT-PET (2.31 ± 1.32 mm vs. 4.12 ± 3.00 mm), underscoring both the distinct motion patterns and the specific challenges of upright imaging.

Conclusions The upright WT-PET scanner presents distinct motion control challenges in clinical practice. This study demonstrates that combining ergonomic supports with breath-holding protocols can effectively reduce patient motion during upright PET imaging; however, a full 30-s breath-hold is not feasible for 70% of patients. Since 50% of patients were able to perform a moderate breath-hold, a two-step acquisition can be performed, each comprising 15 s. Moreover, including a healthy volunteer control group and comparisons with conventional PET confirm both the feasibility and the current limitations of the WT-PET.

Keywords Motion tracking, Walk-through PET, Infrared-based localization, Upright imaging, Breath-holding

Introduction

Patient motion remains a persistent challenge in positron emission tomography (PET), as it can cause inconsistencies in projection data and lead to reconstruction artifacts. Longer acquisition times increase the likelihood of such motion, degrading image quality and impairing the accurate characterization and quantification of radiotracer uptake in target tissues. Motion in PET imaging can generally be classified as voluntary and involuntary motion. Voluntary motion includes intentional or uncontrolled movements of the head, jaw, limbs, or larger body segments, often due to muscle activity [1, 2]. Involuntary motion, on the contrary, encompasses a range of physiological movements, such as respiratory-induced thoracic and abdominal motion [3, 4], cardiac motion [4, 5], and peristalsis [6].

While breath-hold imaging protocols can help minimize respiratory motion, typically by acquiring data at end inspiration or end expiration, these techniques are limited to short durations of less than one minute [7]. In combined PET/CT imaging, a fast, free-breathing CT scan is typically followed by a slower, free-breathing PET acquisition, during which respiratory motion can cause significant misalignment between the two modalities. Such misalignment leads to attenuation correction errors and quantification biases in the reconstructed PET images [8]. Motion-induced artifacts, including image blurring or loss of contrast, are particularly problematic in high-resolution and high-sensitivity PET systems where image precision is essential.

Various techniques have been proposed to mitigate respiratory motion artifacts, including prone positioning [9], rescanning, and data-driven respiratory gating [10]. More recently, deep learning (DL)-based approaches have shown promise in reducing motion-induced artifacts and improving attenuation correction [11–13], especially when combined with time-of-flight PET data [14–16]. However, these computational strategies often add operational complexity and increase reconstruction times, posing challenges for seamless clinical integration [15]. In contrast, breath-hold techniques may offer a practical and low-complexity alternative (or complement) to computational methods, particularly in systems where shorter acquisition times make breath-holding feasible.

One such system is the Walk-Through PET (WT-PET) scanner, which introduces a novel design inspired by flat-panel airport scanners, where the patient stands upright between two flat detector panels. These panels, measuring 106 cm in height, 71 cm in width, and spaced 50 cm apart, cover the head and torso to the upper thigh, as represented by Fig. 1a. The compact dimensions of the WT-PET mock-up scanner (2.3 m

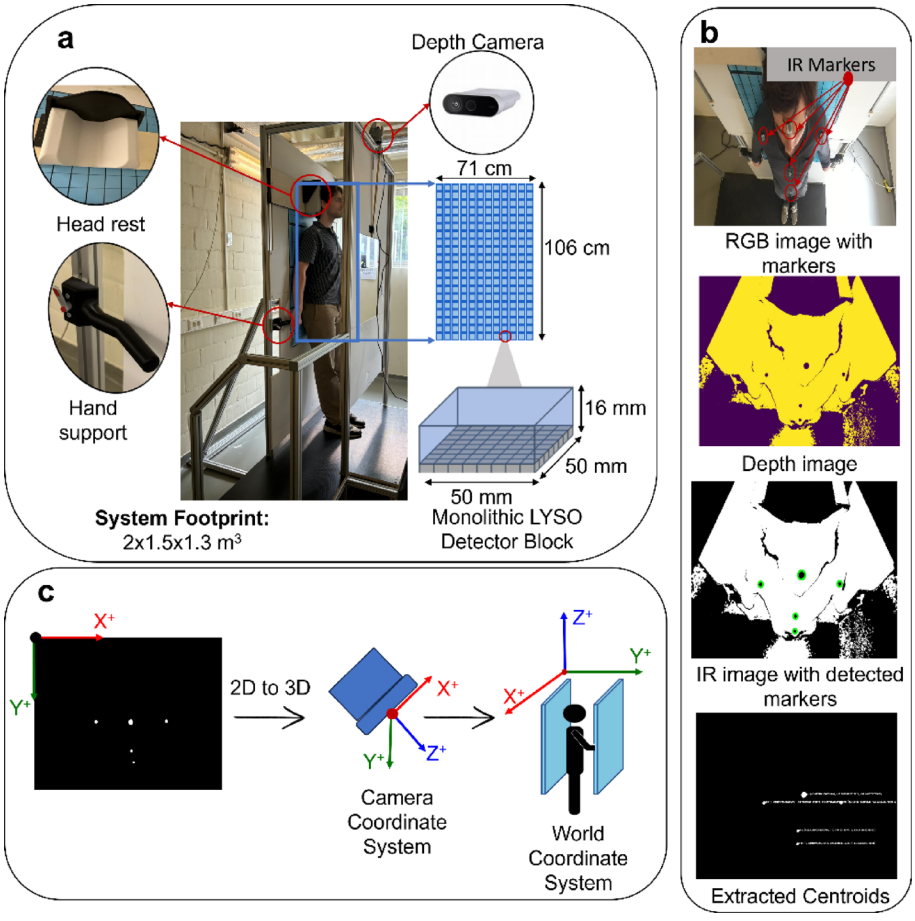

Fig. 1 WT-PET system setup, image processing, and coordinate transformation **a** system setup: overview of the walk-through PET prototype with motion tracking setup. The system features a depth camera mounted on top of the front detector panel at a ~ 45° downward angle, a headrest, and hand supports designed to minimize patient motion and aid standing posture during scanning. The detector panel consists of multiple monolithic LYSO crystal blocks ($50 \times 50 \times 16$ mm^3), each optically coupled to SiPM photodetectors, as illustrated in the schematic zoom. (b) Image Processing: Infrared (IR) markers on the body are tracked using thresholding, connected component analysis, and centroid calculation. (c) Coordinate Transformation: 2D IR marker centroids are converted into 3D world coordinates, aligning the depth camera's local frame with the scanner geometry. Axes orientations (X^+, Y^+, Z^+) illustrate the transformation

height × 2.0 m width × 1.5 m depth; see Fig. 1a) offer a substantially smaller footprint compared to conventional PET scanners, making it suitable for more flexible clinical environments. Each detector block is composed of a monolithic lutetium-yttrium oxyorthosilicate (LYSO) scintillator ($50 \times 50 \times 16$ mm^3) coupled to a silicon photomultiplier (SiPM) array. This design enables high-resolution, depth-sensitive detection, as schematically illustrated in Fig. 1a. Leveraging LYSO detectors with depth of interaction (DOI) technology, the WT-PET system aims to achieve a spatial resolution of up to 2 mm [17–19]. This innovative detector design and the inclusion of DOI technology allow for closer positioning of the panels to the patient, significantly reducing the number of required detectors and lowering costs by approximately 50% compared to the cylindrical long axial field of view (LAFOV) PET systems with equivalent sensitivity and axial field of view (AFOV). Furthermore, time-of-flight (TOF) technology enhances adequate sensitivity, enabling high-quality imaging with fewer counts. In monolithic LYSO detectors,

TOF resolution typically ranges from 200 to 300 ps, further improving image reconstruction efficiency [20].

In addition to its cost efficiency, the WT-PET scanner optimizes patient throughput and positioning. Patients can easily step into the scanner and position themselves using an ergonomically designed headrest and hand support for stability. The scanner's high sensitivity enables a short scan duration of 30 s, reducing overall throughput time to approximately 2–4 min. Routine clinical practice employs list-mode acquisition, particularly for brain PET in patients with dementia, to allow retrospective motion correction in case of patient movement. By combining rapid scanning with ergonomic supports, the WT-PET scanner offers a streamlined workflow that may enhance both patient comfort and operational efficiency [20, 21].

However, upright positioning of patients in the WT-PET presents unique motion challenges. Our previous studies showed increased motion susceptibility in upright imaging using infrared (IR)-based tracking, both in healthy volunteers [21–25] and patients [20]. In a clinical setting, patients of certain ages and clinical indications may have motions that differ significantly from those seen in healthy volunteers, necessitating further investigation. While short scan durations and breath-hold techniques can reduce respiratory motion, patient tolerance varies, and motion can still occur toward the end of prolonged breath-holds; moreover, patient compliance with breath-hold instructions is not guaranteed, which can significantly affect motion outcomes, suggesting that shorter or segmented breath-hold strategies may improve effectiveness.

This work presents two complementary motion studies: one involving a patient study using both a WT-PET mock-up and a conventional cylindrical PET system, and another involving healthy volunteers scanned on both systems. These studies compare motion patterns between upright and supine imaging geometries, assess the effect of breath-hold on motion reduction, and explore demographic influences such as age, BMI, and gender. The findings aim to inform motion mitigation strategies and evaluate the feasibility of upright PET imaging in clinical practice.

Materials and methods

Participant characteristics and experimental framework

This motion study involved two distinct populations, i.e., patients and healthy volunteers, across two different PET scanner configurations, including a WT-PET mock-up scanner and a standard cylindrical PET scanner.

WT-PET patient study

This motion study was conducted at the University Hospital of Liège Nuclear Medicine Department, following approval from the Liège University Hospital-Faculty Ethics Committee (number: B7072022000034, EudraCT 2022-002995-35) on October 2nd, 2024, including 30 patients. Written informed consent was obtained from all participants.

Consecutive patients scheduled for PET scans on October 2, 2024, were invited to participate. Of these, 23/30 (77%) were referred for 2-deoxy-2-[^{18}F] fluoro-D-glucose ([^{18}F] FDG) PET and 7/30 (23%) for prostate-specific membrane antigen radioligand ([^{68} Ga] Ga-PSMA-11) PET. Patient selection was based on willingness to participate, ensuring the inclusion of individuals able to stand upright in the WT-PET mock-up. Out of 45 patients invited, 30 consented to participate, resulting in a 67% participation rate. Of

the 15 patients who did not participate, reasons included refusal to consent (n = 4), hospitalization and confinement to bed (n = 5), use of a wheelchair (n = 2), technical issues (n = 1), language barrier (n = 1), administrative oversight during scheduling (n = 1), and ineligibility due to age (child; n = 1).

The cohort included 12 (40%) patients with no history of malignancy and no malignant findings on PET/CT, who were scanned for benign indications such as lung nodule characterization, follow-up of non-malignant lesions (e.g., solid pseudopapillary tumor of the pancreas), or inflammatory conditions. Six patients (20%) had a history of cancer but no current malignant findings, including individuals with prior breast, lung, or prostate cancer in remission. Twelve patients (40%) had active malignancies, including 8 patients (27%) with metastatic disease. All patients had an Eastern Cooperative Oncology Group (ECOG) performance status of 0–1, indicating they were fully active or restricted in physically strenuous activity but ambulatory. This cohort reflects a spectrum from healthy individuals to patients with active or treated malignancies, enabling evaluation of motion and PET imaging feasibility across diverse clinical profiles. Demographic and clinical details are summarized in Table 1.

Cylindrical PET patient study

To provide a comparison with standard PET geometry, we included a cohort of 13 patients from a previously published study who underwent routine PET/CT examinations on a standard cylindrical PET scanner (Siemens Biograph Vision 600, University Hospital of Liège) [21]. Motion tracking was performed under normal breathing instructions using a similar infrared marker setup as used in the WT-PET study. These patients were independent from those included in the WT-PET cohort, and written informed consent was obtained from all participants (study approved by the institutional Ethics Committee of the CHU of Liege; number: B7072022000034; EudraCT

Table 1 Patient demographics and clinical data

Demographics and clinical data	**Value**	**Range**
Total Patients, n (%)	30 (100%)	–
Male, n (%)	20 (67.0%)	–
Female, n (%)	10 (33.0%)	–
Mean age ± SD (years)	63.5 ± 13.9	29–80
Mean height ± SD (cm)	170.6 ± 8.8	157–190
Mean BMI ± SD (kg/m^2)	28.2 ± 6.5	19.5–44.0
BMI categories	**Patients, n (%)**	**BMI range (kg/m^2)**
Normal Weight	11 (36.7%)	18.5–24.9
Overweight	7 (23.3%)	25.0–29.9
Obese	12 (40.0%)	≥ 30
Breath-hold categories	**Patients, n (%)**	**Time (s)**
Full Breath-hold	9 (30.0%)	30
Moderate Breath-hold	15 (50.0%)	20–29
Short Breath-hold	6 (20%)	> 20
Primary diagnosis		**Patients, n (%)**
No malignancy		12 (40%)
History of cancer, and:		18 (60%)
No Malignant findings		6 (20%)
Limited-stage or low-grade cancer group		4 (13%)
Metastatic disease		8 (27%)

SD standard deviation

2022-0992995-35). Detailed demographic and clinical data have not been collected for this cohort.

Healthy volunteer study (WT-PET and cylindrical PET)

To provide a healthy control reference dataset, 12 healthy volunteers were recruited and scanned at the Ghent University Hospital on both scanner types, i.e., the WT-PET mock-up scanner and cylindrical PET scanner (Siemens mCT). According to institutional guidelines, no ethical approval was needed for this study because it posed little risk and did not gather any personally identifiable health information. All healthy volunteers provided written informed consent before participation.

All healthy volunteers were free of known diseases, capable of complying with breath-hold instructions, and able to remain standing during the 30-s scan. Their demographic characteristics are provided in Table S1 (Supplementary Material). Table 2 summarizes the number of participants, scan durations, and anatomical marker placements for each group scanned with either the WT-PET or Cylindrical PET system.

For all motion analyses, data from the WT-PET patient cohort (n = 30) were used to evaluate marker displacement under normal breathing and all breath-hold instructions. The cylindrical PET patient cohort (n = 13) served as a reference for normal breathing motion in a standard scanner geometry. Data from the 12 healthy volunteers (Table S1), scanned on both WT-PET and cylindrical PET systems, provided a control dataset to compare motion patterns between patients and healthy individuals. This design allowed us to assess the effects of scanner type, breathing instructions, and participant health status on motion magnitude and variability across anatomical markers.

Study design

This study was designed to evaluate upper body motion during PET imaging using infrared marker tracking under controlled breathing instructions across two scanner configurations: a WT-PET mock-up scanner and a standard cylindrical PET scanner. Both patients and healthy volunteers were included, enabling cross-comparison between clinical and non-clinical populations.

All participants scanned with the WT-PET system completed two standardized motion protocols as mentioned in Table 1:

- Normal breathing
- Breath-hold (target duration: 30 s)

While healthy volunteers reliably achieved full breath-hold duration, variability was observed among patients. Therefore, WT-PET patients were stratified into three groups based on actual breath-hold duration:

Table 2 Overview of study groups included in the motion analysis

Study groups	Number of participants	Scan duration	Markers placement
WT-PET patients	30	30 s	Head, shoulders, chest, and abdomen
Cylindrical PET patients	13	8 min	Head, chest, and abdomen
WT-PET volunteers	12	30 s	Head, shoulders, chest, and abdomen
Cylindrical PET volunteers	12	8 min	Head, chest, and abdomen

The table summarizes the number of participants, scan duration, and anatomical marker placements for each group scanned with either the walk-through PET (WT-PET) or the cylindrical PET system

- *Full breath-hold*: Patients who were able to hold their breath for the entire 30-s scan duration (t = 0 s to 30 s).
- *Moderate breath-hold*: Patients who were able to hold their breath for 20–29 s, with the breath-hold assumed to begin at t = 0 s unless stated otherwise.
- *Short breath-hold*: Patients who were able to hold their breath for less than 20 s during the scan.

Unlike patients, healthy volunteers were not grouped by breath-hold duration; instead, their data were analysed as a single group to provide reference motion characteristics under breath-hold instructions.

A separate patient cohort (n = 13) was retrospectively included from routine clinical PET/CT scans performed on a standard cylindrical PET scanner under normal breathing instructions. These scans followed standard clinical protocols with a total scan duration of 8 min. Infrared motion tracking was applied during this time using a similar marker configuration. Additionally, a paired dataset of 12 healthy volunteers was acquired on both scanners (WT-PET and cylindrical PET).

Motion tracking setup

Following informed consent, five passive infrared (IR) markers were attached to anatomical positions: head, left shoulder, right shoulder, chest, and abdomen, to enable 3D motion tracking. This full five-marker configuration was consistently applied across the WT-PET patient and healthy volunteer studies. For the cylindrical PET study, however, a simplified marker setup was implemented due to practical limitations. Specifically, two markers were placed on the chest (later averaged during analysis), with additional markers on the head and abdomen (Table 2) as can be seen in Fig. 2a.

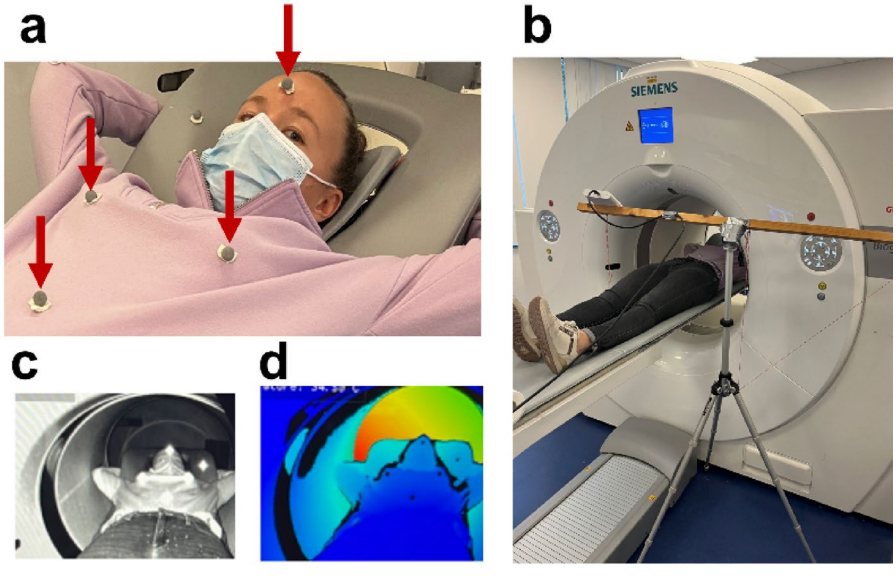

Fig. 2 Illustration of participant (not a true participant in the figure) positioning and motion tracking setup on the conventional cylindrical PET scanner. **a** Placement of infrared markers, **b** positioning of the depth camera above the scanner bed, **c** sample infrared image showing marker visibility, and **d** corresponding depth image used for 3D motion analysis

All markers were positioned within the scanner's field of view (FOV) and tracked using an Orbbec Femto Mega depth camera configured in narrow FOV unbinned mode (640 × 576 pixels). The camera was mounted at the top of the front WT-PET scanner panel, angled downward to ensure optimal visibility of all markers (Fig. 1a).

During the WT-PET scan procedure, participants stood upright in the WT-PET mock-up scanner, with individualized adjustments made to the headrest and hand supports to ensure maximum stability. For each participant, two 30-s video recordings were acquired under different breathing instructions. Each recording captured synchronized RGB, infrared (IR), and depth streams for motion analysis. The acquisition was immediately stopped at the end of the breath-hold period to prevent capturing post-breath-hold movement.

In contrast, the patient study on the standard cylindrical PET scanner utilized a Microsoft Azure Kinect system, acquiring depth video at 15 frames per second for motion tracking under similar conditions. The depth camera was placed in front of the scanner, as can be seen in Fig. 2b. Moreover, a sample infrared and depth image on a cylindrical PET scanner is represented by Fig. 2c, d.

Image processing pipeline

The infrared image processing pipeline follows a similar approach to previous motion studies [25], incorporating thresholding, connected component analysis, centroid calculation, 2D-to-3D transformation, and coordinate conversion (Fig. 1b, c).

Quantification of motion

Motion profile analysis

To evaluate temporal motion characteristics during PET acquisition, average motion profiles were computed for each anatomical marker across participants. For each subject, three-dimensional motion trajectories (X, Y, Z) were extracted for all the markers. These trajectories were first aligned in time, and all frames were either trimmed or padded to match the duration of the longest sequence in the cohort, ensuring consistent frame count across participants. For each marker and axis, motion data were then stacked across participants, and the mean and standard deviation were calculated at each time point to generate population-level motion profiles. Final results were plotted as mean ± standard deviation motion curves, providing insight into both the magnitude and variability of motion over time.

Average absolute deviation analysis

The average absolute deviation (AAD) was calculated for each marker's coordinate (x, y, z) to quantify motion. The AAD values were then compared between the normal breathing and breath-holding instructions. The average absolute deviation (AAD) in each spatial direction (X, Y, Z) was computed as:

$$AAD = \frac{1}{n}\sum_{i=1}^{n}\begin{bmatrix} |x_i - \overline{x}| \\ |y_i - \overline{y}| \\ |z_i - \overline{z}| \end{bmatrix} \tag{1}$$

Here, x_i, y_i, and z_i represent individual coordinate values. $\overline{x}, \overline{y}, \text{ and } \overline{z}$ are the mean values of the respective coordinates, and n is the total number of coordinate values.

Euclidean distance analysis

The extent of motion for each marker is further quantified by calculating the 3D Euclidean distance (ED) from its mean position averaged over all frames, as defined in Eq. 2. This metric provides a straightforward and interpretable measure of rigid body displacement and is well-suited to the infrared marker-based tracking system used in this study. While it does not capture rotational or non-rigid deformations, ED effectively reflects overall motion magnitude and can serve as an indicator of differences between breathing instructions or scanner types. We note, however, that ED may be influenced by individual variability in breathing patterns or anatomy, and should be interpreted with caution when comparing across participants.

$$\mathrm{d} = \sqrt{\frac{1}{\mathrm{n}}\sum_{\mathrm{i}=1}^{\mathrm{n}}[(\mathrm{x_i}-\overline{\mathrm{x}})^2+(\mathrm{y_i}-\overline{\mathrm{y}})^2+(\mathrm{z_i}-\overline{\mathrm{z}})^2]} \tag{2}$$

Impact of breathing instructions on motion in WT-PET patients

To quantitatively compare motion under normal breathing and breath-hold instructions across all marker positions, we first assessed the normality of the data for each marker using the Shapiro–Wilk test based on the Euclidean distance data. This test was conducted to determine whether parametric or non-parametric statistical methods were appropriate for subsequent comparisons. If the data followed a normal distribution, a parametric paired t-test was applied; otherwise, a non-parametric Wilcoxon signed-rank test was used, as it does not assume normality and is more appropriate for skewed or non-normally distributed data.

Demographics influence on WT-PET patient motion: age, BMI, and gender

Motion data for each marker was analyzed individually within each breathing condition. The respective test statistic and its corresponding p value were computed for each marker. A significance level of $p < 0.05$ was used to identify statistically significant differences.

Spearman correlation coefficients were used to assess the relationship between motion data and both age and BMI. This non-parametric method was selected due to the non-linear nature and non-normal distribution of the motion data, as well as its robustness to outliers.

For gender-based comparisons, normality was first evaluated using the Shapiro–Wilk test. Depending on the distribution, either a parametric unpaired t-test or a non-parametric Mann–Whitney U test was applied to assess differences in motion across all marker positions under both normal breathing and breath-hold instructions.

Results

Motion analysis in WT-PET patients

Temporal motion profiles and euclidean distance analyses of WT-PET patients

Figure 3 presents group-averaged motion profiles (X, Y, Z) with standard deviation bands for five anatomical markers (abdomen, chest, head, left shoulder, right shoulder) under normal breathing and three breath-hold durations (short, moderate, full). Motion was generally limited during normal breathing, with the largest variability in abdomen

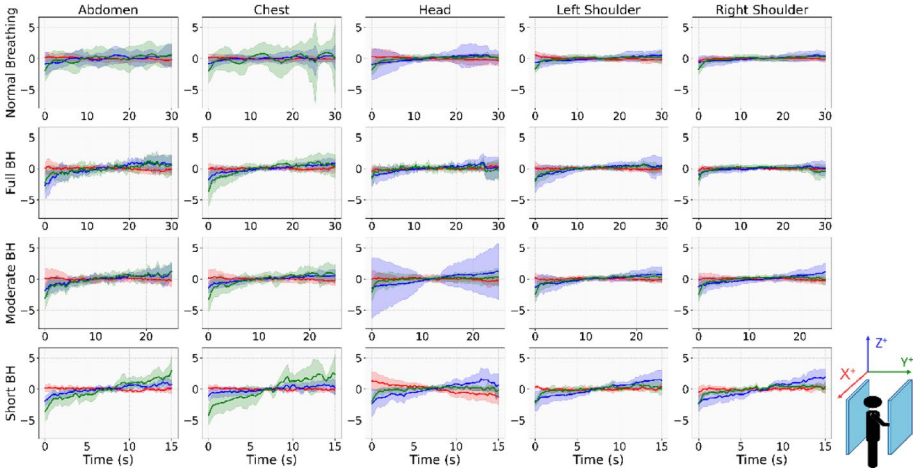

Fig. 3 Group-averaged motion profiles with standard deviation bands for five anatomical markers (abdomen, chest, head, left shoulder, and right shoulder) under four breathing instructions (normal breathing, full breath-hold, moderate breath-hold, and short breath-hold). Each subplot shows the mean motion (solid lines) in the X (red), Y (green), and Z (blue) directions, with shaded areas representing standard deviation across participants

Table 3 Average absolute deviation with standard deviation for normal breathing and breath-holding averaged over all participants

Marker position	Direction	Normal breathing AAD ± SD (mm)	Breath-holding AAD ± SD (mm)
Head	X	0.479 ± 0.512	0.521 ± 0.515
	Y	0.518 ± 0.250	0.687 ± 0.494
	Z	1.058 ± 2.310	1.053 ± 1.774
Left Shoulder	X	0.424 ± 0.390	0.372 ± 0.161
	Y	0.518 ± 0.250	0.624 ± 0.378
	Z	0.924 ± 1.138	0.870 ± 0.725
Right Shoulder	X	0.378 ± 0.263	0.380 ± 0.278
	Y	0.544 ± 0.445	0.541 ± 0.336
	Z	0.893 ± 1.048	0.700 ± 0.657
Chest	X	0.464 ± 0.246	0.484 ± 0.270
	Y	1.672 ± 1.574	1.215 ± 0.832
	Z	0.780 ± 0.546	0.658 ± 0.387
Abdomen	X	0.618 ± 0.333	0.594 ± 0.312
	Y	1.574 ± 1.114	1.160 ± 0.654
	Z	1.138 ± 0.716	0.867 ± 0.474

and chest, while head and shoulder markers remained relatively stable. Breath-holding reduced motion, particularly in Y and Z directions, as confirmed by average absolute deviation (Table 3).

Analysis of average absolute deviation (AAD, Table 3) confirmed that breath-holding reduced motion, particularly in the Y and Z directions for the chest (Y: 1.215 ± 0.832 mm; Z: 0.658 ± 0.387 mm) and abdomen (Y: 1.160 ± 0.654 mm; Z: 0.867 ± 0.474 mm), with similar reductions in the Z direction for head and shoulders (Table 3). Standard deviations of AAD decreased in vertical motion, indicating improved stability. For some markers, minor increments occur in X and Y, but overall trends indicate enhanced motion control during breath-hold.

Breath-holding reduced motion across all markers, most prominently in the chest and abdomen, where both mean amplitude and variability decreased relative to normal breathing. Figure 4a shows violin plots of ED for all five markers comparing normal

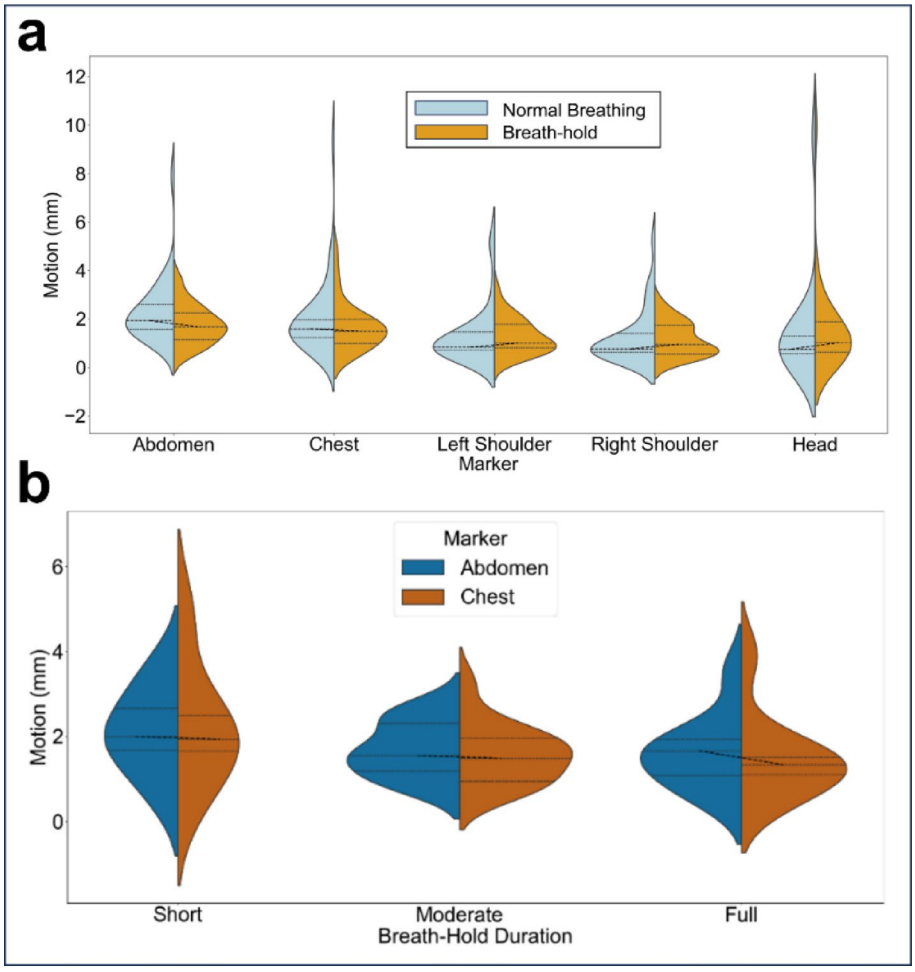

Fig. 4 **a** Distribution of motion across anatomical markers under normal breathing and breath-hold instructions. Violin plots show the Euclidean distance (ED) in millimeters for five markers: abdomen, chest, left shoulder, right shoulder, and head. Blue violins represent motion during normal breathing; orange violins represent breath-hold. Each violin depicts the distribution across participants, with dashed lines indicating the quartiles. Black dashed connectors show the difference between the medians of each condition per marker. **b** Violin plots showing Euclidean motion magnitude (in mm) of the abdomen and chest markers across different breath-hold durations. Motion is compared for short (10–20 s), moderate (20–30 s), and full (30 s) breath-hold strategies

breathing and breath-hold. Reduced motion amplitude and inter-individual variability are evident, particularly for the abdomen (median 1.8 to 1.6 mm) and chest (2.3 to 1.8 mm), while head and shoulder motion remained low (< 1.2 mm). Average ED values are listed in Table S2, showing a decrease in chest values from 2.08 ± 1.66 mm to 1.68 ± 0.99 mm, and the abdomen from 2.31 ± 1.32 mm to 1.76 ± 0.81 mm.

In addition, a violin plot comparing the Euclidean motion amplitudes of the chest and abdomen markers under short, moderate, and full breath-hold instructions is shown in Fig. 4b. The motion magnitude decreased slightly with longer breath-hold durations for both abdomen and chest markers, with the most pronounced reduction observed in the abdomen. For short breath-holds, chest motion exhibited slightly higher overall variability (mean = 2.25 mm, SD = 1.45 mm) than the abdomen (mean = 2.12 mm, SD = 1.03 mm), whereas the abdomen showed a marginally wider interquartile range (0.99 mm vs 0.83 mm), indicating subtle differences in distribution shape between thoracic and diaphragmatic movement. As breath-hold duration increased, median abdominal motion

decreased from 2.00 mm to 1.55 mm (moderate) and 1.66 mm (full), while the spread of the distribution progressively narrowed (IQR = 0.99 to 1.13 and 0.85 mm), suggesting more stable positioning. Chest motion showed a similar but less pronounced trend, with median values decreasing from 1.93 to 1.49 mm and 1.34 mm, consistent with reduced respiratory influence and improved upper-thoracic stability during longer breath-holds. While both moderate and full breath-holds reduced abdominal motion compared to short breath-holds. The lowest median motion was observed in the moderate group, while the full breath-hold condition showed a slightly higher median but a narrower spread, suggesting improved motion consistency rather than further reduction in amplitude.

Figure 5 presents scatter plots comparing normal breathing versus breath-hold ED for all markers, with semi-transparent ellipses representing ± 1 SD around group means. Most points are found below the diagonal for the abdomen and chest, confirming that breath-holding reduces motion, while head and shoulder motion remained low but occasionally variable, reflecting minor postural adjustments or involuntary activity. Color-coded ellipses indicate short (red), moderate (green), and full breath-hold (blue) durations, highlighting that longer breath-holds generally lead to more consistent motion reduction. Overall, motion distances were higher during normal breathing, particularly in the abdomen and chest, showing the most pronounced and consistent reductions during breath-hold, particularly within the full and moderate duration groups.

Demographics influence on WT-PET patient motion: age, BMI, and gender

Normality testing (Table S3) indicated non-normal Euclidean distance distributions for all markers during normal breathing. During breath-hold, the abdomen ($p = 0.268$) and shoulders ($p = 0.055$ and $p = 0{,}007$) approached normality, while head and chest remained non-normal. Given these results, Wilcoxon signed-rank tests were used to compare motion between normal breathing and breath-hold (Table S4). Motion was significantly

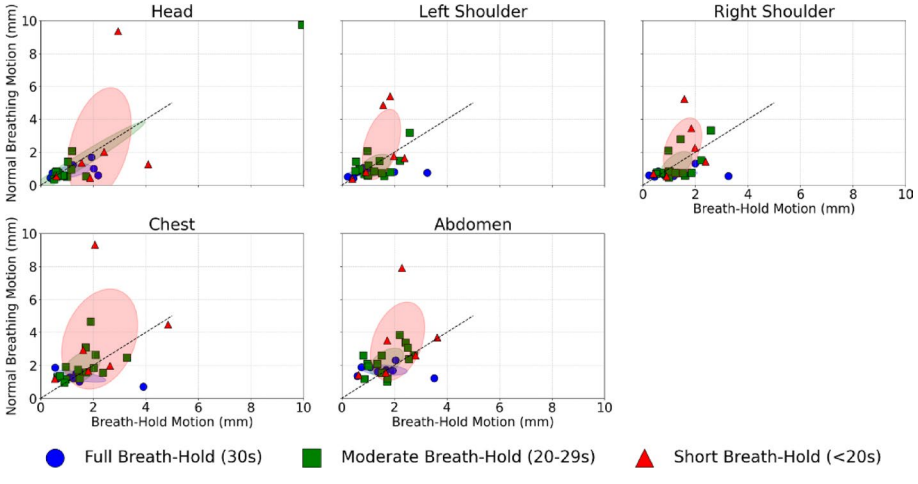

Fig. 5 Scatter plots comparing motion amplitudes of WT-PET patients during breath-hold (x-axis) and normal breathing (y-axis) for five anatomical markers: head, left shoulder, right shoulder, chest, and abdomen. Data points are color-coded by breath-hold duration group (full: blue; moderate: green; short: red). Semi-transparent ellipses denote the 1 standard deviation (SD) region around the group mean, illustrating the distribution and consistency of motion reduction. The red ellipse represents the short breath-hold group, green represents the moderate breath-hold group, and blue represents the full breath-hold group. The dashed identity line indicates equal motion under both conditions; points below this line reflect reduced motion during breath-hold

reduced in the abdomen ($p = 0.005$), while differences for head, chest, and shoulders were not significant ($p > 0.13$).

Demographic analysis (Tables S5–S6) showed that head and right shoulder are significantly correlated with age under both breathing conditions. The reason for this effect on the right shoulder is unclear, but it may reflect individual differences in posture, habitual arm use, or subtle asymmetries in muscle tone; however, the left shoulder did not show a corresponding correlation, so this finding should be interpreted with caution. No consistent correlations were observed for BMI, and Mann–Whitney U-tests revealed no significant gender differences across markers or breathing conditions.

Motion differences between patients and healthy volunteers in WT-PET and the cylindrical PET

Figure 6a compares ED distributions between patients (n = 32) and healthy volunteers (n = 12) under normal breathing and breath-hold. Patients exhibited higher motion in the abdomen, chest, and head, while volunteers demonstrated more consistent stability. Breath-hold reduced motion in both groups, but patients showed variability in motion

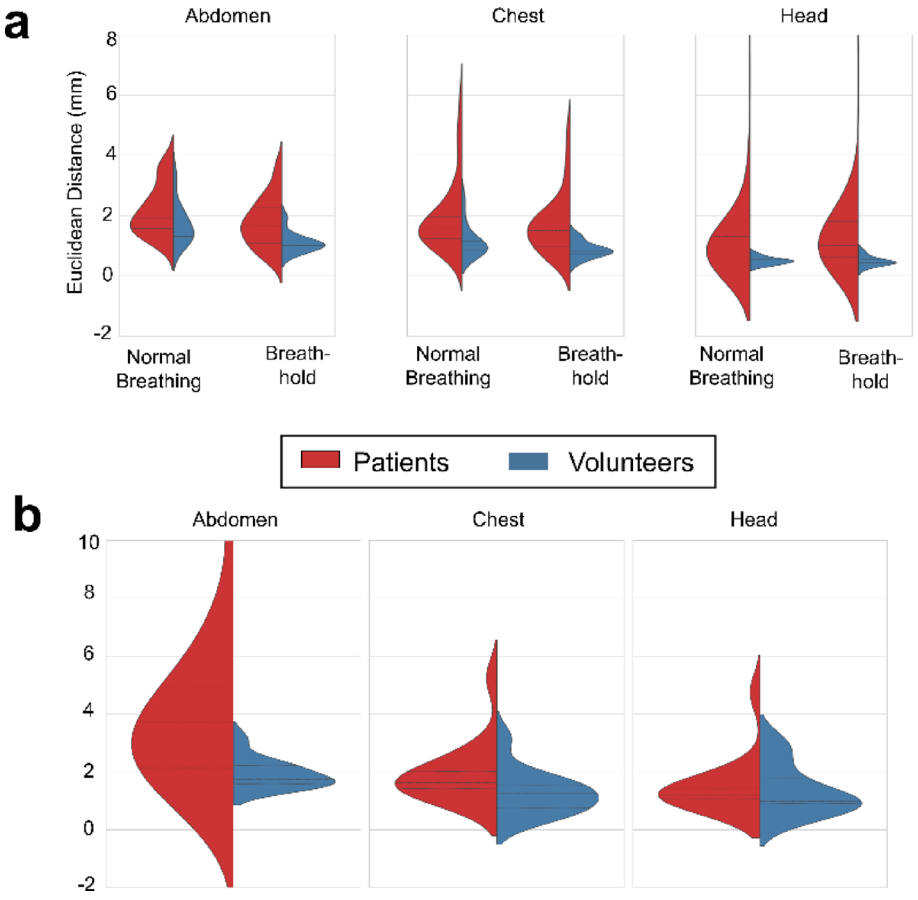

Fig. 6 **a** Violin plots showing the distribution of mean Euclidean motion distances (in mm) across three anatomical markers (abdomen, chest, and head) for patients (n = 32, red) and healthy volunteers (n = 12, blue) under normal breathing and breath-hold instructions. Each plot illustrates the variability and central tendency of marker motion within each group. **b** Distribution of motion (Euclidean distance) for abdomen, chest, and head markers on a standard cylindrical PET scanner. Violin plots show the distribution of mean Euclidean distance (mm) for patients (n = 13, red) and healthy volunteers (n = 12, blue) across three anatomical regions. Each violin illustrates the density of participant-level motion estimates, with internal bars indicating the interquartile range and median

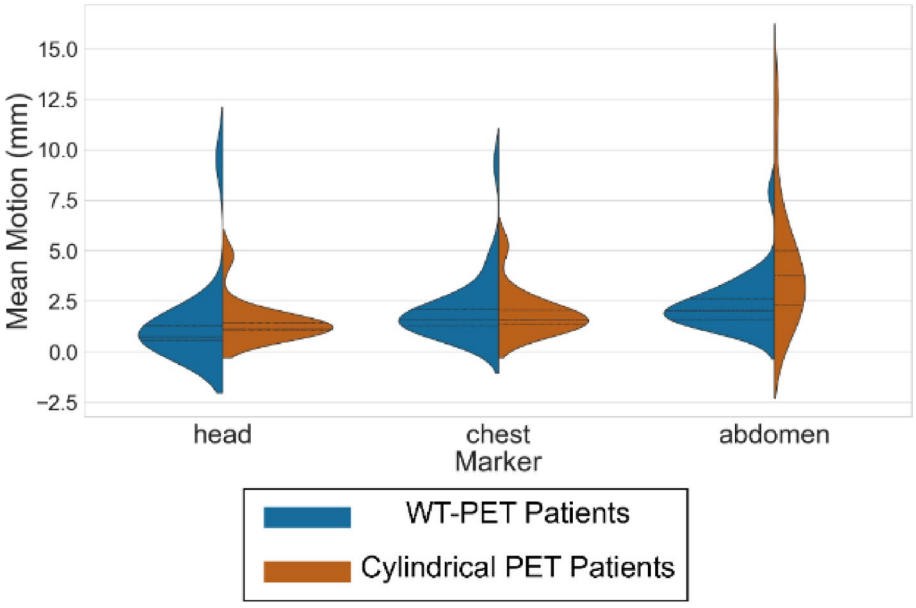

Fig. 7 Violin plots comparing mean motion amplitudes at key anatomical positions between upright WTF-PET and conventional cylindrical PET. WT-PET shows reduced motion, particularly at the abdomen marker, indicating improved stability in these regions with the use of ergonomic supports and breath-hold protocols

as compared to healthy volunteers, particularly in the upper body. Mann–Whitney U tests (Table S7) confirmed significantly higher motion in patients for head, shoulders, and chest markers, while abdominal motion was comparable.

Figure 6b presents ED distributions on a standard cylindrical PET scanner for the abdomen, chest, and head markers. Shapiro–Wilk tests indicated non-normal distributions for most markers (Table S8). Consequently, group differences were assessed using Mann–Whitney U tests (Table S9) and patients exhibited significantly higher abdominal motion ($p = 0.0061$).

To evaluate differences in motion characteristics across scanner types, we compared mean marker motion in WT-PET patients (n = 30) and patients scanned on a conventional cylindrical PET system (n = 12). Three anatomical regions were assessed: head, chest, and abdomen. As shown in Fig. 7, violin plots illustrate the distribution of motion for each marker across both scanner configurations.

Quantitative comparisons were performed using the Mann–Whitney U test (Table S10). Abdominal motion comparisons between WT-PET and conventional PET patients (Table S10) were performed under full breath-hold conditions to ensure consistent assessment of respiratory motion. Abdominal motion was significantly lower in WT-PET patients compared to those in the conventional PET group ($U = 321.0$, $p = 0.0342$), despite the upright positioning in WT-PET. No statistically significant differences were observed in chest motion ($U = 309.0$, $p = 0.0645$) or head motion ($U = 188.0$, $p = 0.3505$). These findings suggest that WT-PET, despite its open design, does not introduce increased motion compared to standard PET and may even provide motion advantages in abdominal regions.

Discussion

This study builds upon earlier investigations involving the initial WT-PET mock-up [21] and subsequent work using an upgraded WT-PET prototype with headrest and hand supports in healthy volunteers [25]. The latter demonstrated that motion in upright healthy subjects was comparable to that observed in conventional cylindrical PET scanners, where participants lie supine. In the present work, we evaluated motion in the upgraded WT-PET prototype in a real-world clinical population.

The results show that the addition of headrest and hand supports can reduce motion in patients. However, compared with healthy volunteers, patients exhibited greater variability in motion, particularly during breath-hold, and motion suppression was less consistent, highlighting the challenges of applying upright PET imaging protocols in individuals with respiratory or mobility limitations.

Statistical analysis revealed that age was significantly correlated with motion, particularly in the head and shoulders during normal breathing, suggesting that older patients may have more difficulty maintaining stillness. Increased head motion was observed in some older patients, likely due to challenges in maintaining upright posture. In Fig. 5, the two patients with the highest motion, outside the standard deviation region, were a patient diagnosed with polyneuropathy and the oldest patient (80 years), respectively. Gender and BMI showed no significant association with motion, indicating that these demographic variables may not be primary determinants of motion stability in upright imaging.

Breath-holding reduced motion magnitude in both the chest (by ~ 20%) and abdomen (by ~ 24%), confirming its value as a motion-suppression strategy. However, a substantial number of patients were unable to tolerate long breath-hold durations. Despite this, breath-hold duration was inversely associated with Euclidean displacement, supporting the notion that longer breath-holds provide improved motion stability. The motion observed during normal breathing was non-normally distributed across all markers, indicating substantial inter-patient variability in respiratory motion. In contrast, breath-holding induced more consistent and normally distributed motion patterns, particularly in the abdomen and shoulders. These findings highlight the benefit of breath-holding not only in reducing motion magnitude but also in enhancing motion uniformity across participants. From a clinical perspective, reducing abdominal motion is particularly beneficial in imaging applications that are highly sensitive to respiratory artifacts [26].

Motion in the head and shoulders remained relatively stable and was minimally affected by respiratory effort, likely due to the mechanical support provided by the headrest and hand grips. However, even small head displacements can degrade image quality, especially in high-resolution PET systems or in head/neck imaging applications. Head motion, in particular, remains a critical confounder in PET imaging, especially in upright configurations like WT-PET. Prior studies have shown that head motion in the upgraded WT-PET mock-up is comparable to that observed in standard cylindrical systems [25]. In the present study, we confirmed this finding through a direct comparison between WT-PET and conventional PET data, which showed no significant difference in head motion between the two systems. Nevertheless, given the higher spatial resolution and increased sensitivity of the WT-PET system, even small head displacements can lead to image blurring and quantification errors. Various correction strategies have been proposed in the literature [2, 27], broadly categorized into hardware-based and data-driven

approaches. Hardware-based techniques often employ external tracking systems, such as the Polaris Vicra (NDI Systems, Waterloo, Canada), which tracks reflective markers affixed to the patient's head in real time at 20 Hz [29]. Marker less variants use surface or facial feature tracking to estimate motion. Data-driven approaches, by contrast, estimate motion directly from the PET data stream [28, 29], offering practical advantages by eliminating the need for external equipment [30]. For clinical translation of WT-PET technology, especially in elderly or neurologically compromised patients, the integration of such correction strategies may be critical.

When comparing patients with healthy volunteers, motion suppression was more consistent and effective in the latter, particularly under breath-hold instructions. This discrepancy likely stems from differences in respiratory control, compliance with instructions, and physical comfort. These findings suggest that even under relaxed breathing instructions, patients tend to move more in the upper body regions, potentially due to discomfort, clinical condition, or reduced ability to remain still. These findings emphasize the need for motion mitigation strategies in clinical imaging workflows.

While breath-holding remains a simple and effective method, it may be insufficient for certain patient groups. Supplemental strategies such as guided breath-hold coaching, instructional videos, or real-time motion feedback may help improve compliance. Furthermore, the elevated variability in chest and abdominal motion among patients suggests the need for adaptive or segmented breath-hold protocols, especially for those with limited capacity to perform long breath-holds. Such tailored approaches could improve image quality, reproducibility, and diagnostic accuracy in upright PET imaging applications.

A direct comparison between WT-PET and conventional cylindrical PET was conducted to assess whether upright imaging introduces additional motion artifacts. Violin plots of mean motion amplitudes (Fig. 6b) across the head, chest, and abdomen revealed that abdominal motion was significantly lower in WT-PET patients, despite the upright positioning ($p = 0.0342$). Head and chest motion did not differ significantly between groups. This suggests that the ergonomic design of the WT-PET system, combined with breath-hold protocols and a shorter acquisition time, may contribute to motion suppression. Importantly, we acknowledge that the WT-PET scans were acquired over 30 s, while conventional PET involved longer (8-min) acquisitions. Notably, abdominal motion in the conventional PET group exhibited higher variability, potentially due to less effective immobilization in the supine position.

There are, however, a few limitations to this study. First, while Euclidean distance (ED) provides a robust and interpretable measure of rigid displacement, it does not capture rotational motion, soft tissue deformation, or local skin movement that may affect PET image quality. Moreover, ED may not fully account for individual differences in breathing patterns (e.g., chest vs. abdominal breathing) or anatomical variability across participants. As such, while ED is useful as a general indicator of motion and instruction compliance, it may not reliably reflect non-compliance or subtle region-specific differences. Future work may benefit from integrating complementary motion descriptors, such as inter-marker distance variability, to assess local deformations [31], centroid or center-of-distribution displacement to quantify global body sway [32], principal component or frequency-domain analyses to separate periodic (respiratory) from irregular motion components [33]. Additionally, using multiple cameras positioned at

complementary angles could improve overall accuracy of motion characterization and 3D reconstruction. Second, although significant motion reductions were observed in the abdomen, several other comparisons yielded non-significant or marginal p-values. These should be interpreted with caution, as statistical power may be limited by the sample size, particularly in stratified subgroup analyses. Expanding the cohort would help validate the observed trends. Third, while breath-hold duration was stratified to account for patient variability, many participants could not sustain a full 30-s breath-hold, limiting the generalizability of this approach. Adaptive or segmented breath-hold protocols may improve feasibility. Finally, comparisons between WT-PET and conventional scanners involved separate cohorts, and differences in age, marker placement, and imaging conditions may introduce variability despite efforts to harmonize procedures. Nonetheless, the inclusion of both patient and healthy volunteer groups across two scanner types provides valuable insight into motion behavior in upright PET imaging.

Conclusion

This study evaluated patient motion in an upright PET imaging setup using the Walk-Through PET (WT-PET) mock-up, testing the addition of ergonomic headrest and hand supports and breath-hold instructions in a clinical population. The findings confirm that breath-holding significantly reduces chest and abdominal motion, and that the WT-PET's ergonomic design offers sufficient stabilization for the upper body. However, the 30-s breath-hold duration was not feasible for over 70% of participants, indicating that shorter breath-hold durations may be more appropriate in clinical practice. Since 50% of patients were able to perform a moderate breath-hold, a two-step acquisition can be performed, each comprising 15 s.

Comparative analysis with conventional PET systems demonstrated that upright imaging does not inherently increase motion and may even reduce abdominal displacement under certain conditions. These results support the clinical viability of WT-PET imaging and point to the value of integrating short-duration breath-hold protocols and real-time motion tracking in future implementations.

Further development should prioritize adaptive acquisition strategies and motion correction methods to accommodate diverse patient needs and ensure consistent image quality across applications.

Supplementary Information

The online version contains supplementary material available at https://doi.org/10.1186/s40658-025-00815-7.

Supplementary Material 1

Acknowledgements

We extend our heartfelt gratitude to all the participants who participated in this study. We also wish to thank the Nuclear Medicine Department of the University Hospital of Liege and Ghent University Hospital for providing the facilities and support necessary to conduct this research. Additionally, we sincerely appreciate the efforts of Comate Engineering for their outstanding work in designing the WT-PET mock-up.

Author contributions

RA conducted the experimental study, drafted the initial manuscript, and contributed to its revision. FM contributed to the conceptual design of the WT-PET mock-up, assisted in conducting the study, especially with patient communication in French, and reviewed the manuscript. NW supported the execution of the study at the Nuclear Medicine Department of CHU Liège Hospital and reviewed the final manuscript. JM provided technical support for the post-processing of the recorded videos and reviewed the manuscript. MD offered mechanical assistance to transport the WT-PET mock-up scanner to Liège. BV reviewed the manuscript. YD supported the execution of the study at the Nuclear Medicine Department of Ghent University Hospital. CV co-supervised the project, provided guidance, and reviewed the manuscript. SV supervised the project, provided overall guidance, and reviewed the manuscript.

Funding
This project has received funding from the FWO (Research Foundation Flanders)-Large-scale research infrastructure and the Sphynx project.

Data availability
Not applicable.

Code availability
Code is available from the corresponding author upon reasonable request.

Declarations

Ethics approval and consent to participate
This study was approved by the Liège University Hospital-Faculty Ethics Committee (CHU Liège, EudraCT 2022-002995-35). Informed consent was obtained from all individual participants included in the study.

Consent for publication
Patients signed informed consent regarding publishing their data.

Competing interests
The authors declare no conflicts of interest.

Clinical trial number
Not applicable.

Received: 26 May 2025 / Accepted: 3 November 2025
Published online: 27 November 2025

References

1. Goldstein SR, Daube-Witherspoon ME, Green MV, Eidsath A. A head motion measurement system suitable for emission computed tomography. IEEE Trans Med Imaging. 1997;16(1):17–27. https://doi.org/10.1109/42.552052.
2. Montgomery AJ, Thielemans K, Mehta MA, Turkheimer F, Mustafovic S, Grasby PM. Correction of head movement on PET studies: comparison of methods. J Nucl Med. 2006;47(12):1936.
3. Nehmeh SA, et al. Effect of respiratory gating on reducing lung motion artifacts in PET imaging of lung cancer. Med Phys. 2002;29(3):366–71. https://doi.org/10.1118/1.1448824.
4. Rubeaux M, Doris MK, Alessio A, Slomka PJ. Enhancing cardiac PET by motion correction techniques. Curr Cardiol Rep. 2017;19(2):14.
5. Sun T, et al. Body motion detection and correction in cardiac PET: phantom and human studies. Med Phys. 2019;46(11):4898–906. https://doi.org/10.1002/mp.13815.
6. Wang J, et al. Motion-correction strategies for enhancing whole-body PET imaging. Front Nucl Med. 2024. https://doi.org/10.3389/fnume.2024.1257880.
7. Kyme AZ, Fulton RR. Motion estimation and correction in SPECT, PET and CT. Phys Med Biol. 2021. https://doi.org/10.1088/1361-6560/ac093b.
8. Hamill JJ, Meier JG, Betancourt Cuellar SL, Sabloff B, Erasmus JJ, Mawlawi O. Improved alignment of PET and CT images in whole-body PET/CT in cases of respiratory motion during CT. J Nucl Med. 2020;61(9):1376–80.
9. Lee HJ, et al. Prone position [18F]FDG PET/CT to reduce respiratory motion artefacts in the evaluation of lung nodules. Eur Radiol. 2021;31(7):4606–14. https://doi.org/10.1007/s00330-021-07894-x.
10. Ren S, Lu Y, Bertolli O, Thielemans K, Carson RE. Event-by-event non-rigid data-driven PET respiratory motion correction methods: comparison of principal component analysis and centroid of distribution. Phys Med Biol. 2019. https://doi.org/10.1088/1361-6560/ab0bc9.
11. Li T, Zhang M, Qi W, Asma E, Qi J. Motion correction of respiratory-gated PET images using deep learning based image registration framework. Phys Med Biol. 2020. https://doi.org/10.1088/1361-6560/ab8688.
12. Toyonaga T, et al. Deep learning–based attenuation correction for whole-body PET — a multi-tracer study with ^{18}F-FDG, ^{68}Ga-DOTATATE, and ^{18}F-Fluciclovine. Eur J Nucl Med Mol Imaging. 2022. https://doi.org/10.1007/s00259-022-05748-2.
13. Schaefferkoetter J, Shah V, Hayden C, Prior JO, Zuehlsdorff S. Deep learning for improving PET/CT attenuation correction by elastic registration of anatomical data. Eur J Nucl Med Mol Imaging. 2023;50(8):2292–304.
14. Lu Y, et al. Respiratory motion compensation for PET/CT with motion information derived from matched attenuation-corrected gated PET data. J Nucl Med. 2018;59(9):1480–6.
15. Lu Y, et al. Deep learning-aided respiratory motion compensation in PET/CT: addressing motion induced resolution loss, attenuation correction artifacts and PET-CT misalignment. Eur J Nucl Med Mol Imaging. 2024;52(1):62–73.
16. Hwang D, Kang SK, Kim KY, Choi H, Seo S, Lee JS. Data-driven respiratory phase-matched PET attenuation correction without CT. Phys Med Biol. 2021. https://doi.org/10.1088/1361-6560/abfc8f.
17. Abi Akl M, Dadgar M, Toufique Y, Bouhali O, Vandenberghe S. Monte Carlo simulation of the system performance of a long axial field-of-view PET based on monolithic LYSO detectors. EJNMMI Phys. 2023;10(1):37.
18. Abi-Akl M, Maebe J, Vervenne B, Bouhali O, Vanhove C, Vandenberghe S. Performance evaluation of a medium axial-field-of-view sparse pet system based on flat panels of monolithic LYSO detectors: a simulation study. EJNMMI Phys. 2025;12:49.
19. Dadgar M, Maebe J, Abi Akl M, Vervenne B, Vandenberghe S. A simulation study of the system characteristics for a long axial FOV PET design based on monolithic BGO flat panels compared with a pixelated LSO cylindrical design. EJNMMI Phys. 2023. https://doi.org/10.1186/s40658-023-00593-0.

20. Vandenberghe S, et al. Walk-through flat panel total-body PET: a patient-centered design for high throughput imaging at lower cost using DOI-capable high-resolution monolithic detectors. Eur J Nucl Med Mol Imaging. 2023. https://doi.org/10.1007/s00259-023-06341-x.
21. Muller FM, Maebe J, Withofs N, Vandenberghe S. Walk-through flat-panel total body PET : system design and comparison of body motion with a standard PET-CT. In: EANM'23, 2023 (Abstract Number: OP-568) https://doi.org/10.1007/s00259-023-06333-x.
22. Muller FM, Maebe J, Dadgar M, Withofs N, Vanhove C., Vandenberge S. Rigid body motion analysis in walk-through total body PET scanner based on real-time motion tracking with cameras: comparative study between free-breathing and breath-hold. In: Total-body PET 2022, 2022.
23. Aziz R, Maebe J, Vandenberghe S. Motion analysis of Subjects standing in walk-through total body PET using infrared based localization. In: PSMR2024 10th conference on PET, SPECT, and MR multimodal technologies, total body and fast timing in medical imaging., May 2024, pp. 62–63.
24. Aziz R, Maebe J, Vervenne B, Muller FM, Withofs N, Vandenberghe S. Exploring motion patterns of subjects on a mock-up walk-through total body PET using infrared localization. In: Total-body PET 2024, 2024.
25. Aziz R, Maebe J, Muller FM, D'Asseler Y, Vandenberghe S. Quantitative analysis of patient motion in walk-through PET scanner and standard axial field of view pet scanner using infrared-based tracking. EJNMMI Phys. 2024;11(1):99.
26. Webster A, Mundora Y, Clark CH, Hawkins MA. A systematic review of the impact of abdominal compression and breath-hold techniques on motion, inter-fraction set-up errors, and intra-fraction errors in patients with hepatobiliary and pancreatic malignancies. Radiother Oncol. 2024;201:110581. https://doi.org/10.1016/j.radonc.2024.110581.
27. Fulton RR, Meikle SR, Eberl S, Pfeiffer J, Constable CJ. Correction for head movements in positron emission tomography using an optical motion-tracking system. IEEE Trans Nucl Sci. 2002;49(1):116–23.
28. Lu Y, et al. Data-driven motion detection and event-by-event correction for brain PET: comparison with vicra. J Nucl Med. 2020;61(9):1397–403.
29. Mukherjee J, et al. Improved frame-based estimation of head motion in PET brain imaging. Med Phys. 2016;43:2443–54.
30. Sun C, et al. An objective evaluation method for head motion estimation in PET—motion corrected centroid-of-distribution. Neuroimage. 2022. https://doi.org/10.1016/j.neuroimage.2022.119678.
31. Merriaux P, Dupuis Y, Boutteau R, Vasseur P, Savatier X. A study of Vicon system positioning performance. Sensors. 2017. https://doi.org/10.3390/s17071591.
32. Spangler-Bickell MG, Hurley SA, Pirasteh A, Perlman SB, Deller T, McMillan AB. Evaluation of data-driven rigid motion correction in clinical brain PET imaging. J Nucl Med. 2022;63(10):1604. https://doi.org/10.2967/jnumed.121.263309.
33. Ashe WB, et al. Analysis of respiratory kinematics: a method to characterize breaths from motion signals. Physiol Meas. 2022. https://doi.org/10.1088/1361-6579/ac4d1a.

Publisher's Note